Supporting Information

Ultrafast synthesis of cation/anion co-doped Li-rich layered oxide cathodes with Li^{+}/Ni^{2+} mixing structural defects

Wei Zhu,[a] *Jiwei Zhao*,[a] *Ming Yang*,*[b] *Jialu Zhan*,[a] *Hai Su*,[a] *Cuihua Zeng*,[a] *Zhenfei Li*,[a] *Jing Zhang*,[b] *Yanan Chen*,*[a] *Yunhua Xu**[a]

[a] School of Materials Science and Engineering, Key Laboratory of Advanced Ceramics and Machining Technology (Ministry of Education), and Tianjin Key Laboratory of Composite and Functional Materials, Tianjin University, Tianjin 300072, China.

[b] Science and Technology on Power Sources Laboratory, Tianjin Institute of Power Sources, Tianjin 300384, China.

*Corresponding author. Email: yangmingnk@163.com (M.Y.); yananchen@tju.edu.cn (Y. C.); yunhua.xu@tju.edu.cn (Y. X.)

Experimental Section

Synthesis of LLO and KP-LLO.

Synthesis of the precursor of LLO ($Li_{1.2}Ni_{0.13}Co_{0.13}Mn_{0.54}O_2$): The precursor of LLO was obtained by mixing $Mn_{4/6}Ni_{1/6}Co_{1/6}CO_3$ ($TMCO_3$) and Li_2CO_3 (mass ratio, $TMCO_3$: Li_2CO_3 = 100 : 49), which was purchased from Jiang su Hai 'an zhichuan battery material technology co., LTD.

Synthesis of the precursor of KP-LLO: The precursor of KP-LLO was obtained by mixing $Mn_{4/6}Ni_{1/6}Co_{1/6}CO_3$ ($TMCO_3$), Li_2CO_3, and KH_2PO_4 (mass ratio, $TMCO_3$: Li_2CO_3 : KH_2PO_4 = 100 : 49 :1.46).

The NFTS process: In this process, the precursor was placed on a nickel foil heater (nickel foil, 5 cm × 2 cm) driven by a DC power supply (MP50100D) in the air atmosphere. Then the precursor was calcined in a two-step process to produce the cathode material, including precalcination (~660 ℃ for ~54 s) and calcination (~970 ℃ for ~43 s). The temperature of the heater can be tuned by adjusting the current and voltage and measured by a laser infrared thermometer (Sanya Kechuang Future Technology).

Carbon-based Joule heating: The process is similar to that of NFTS except that carbon cloth is used as the heating medium.

Materials Characterization.

Inductively coupled plasma-optical emission spectrometry (ICP-OES) was employed to measure the chemical composition of the materials. The crystal structures of the materials were characterized by powder X-ray diffraction (XRD) on a D8 Advanced X-ray diffractometer with Cu Kα radiation at 40 kV and 40 mA. Rietveld refinements of the XRD patterns were obtained using EXPGUI software.[1] The morphologies of the materials were observed by using field emission scanning electron microscopy (FSEM, s4800). X-ray photoelectron spectroscopy (XPS, Axis Supra) was used to analyze the surface chemical properties of the materials, and all the XPS spectra were calibrated with the C 1s peak (284.6 eV). The valence states of Mn ions were calculated using the following equation: AOS=8.956-1.126ΔE (ΔE: the splitting energies between the Mn

3s peak and its satellite peak). Transmission electron microscopy (TEM, JEM-2100F) equipped with an energy dispersive X-ray spectrometer (EDS) was used to observe the microstructures and elemental distributions of the materials. Raman spectra were analyzed using a Raman laser spectrometer (Renishaw) with an excitation wavelength of 532 nm. Fourier transform infrared (FTIR, Alpha II, Germany) spectra was used to investigate the surface structure of the materials. The oxygen release during the initial charging process was detected by operando differential electrochemical mass spectrometry (DEMS, Linglu Instruments (Shanghai) Co., Ltd.).

Electrochemical measurements.

The cathode was prepared by mixing LLO (or KP-LLO) as the active material, polyvinylidene fluoride as the binder, and Super P as the conductive agent in a mass ratio of 8:1:1 into a homogeneous slurry in N-methyl-2-pyrrolidone (NMP) by using magnetic stirrer. The obtained slurry was cast on carbon-coated aluminum foil and vacuum dried at 100 ℃ overnight. Then the dried electrodes cut into circular pieces with a diameter of 9 mm. CR2032 half cells were assembled in an argon-filled glove box using the prepared cathode, microporous polypropylene membrane (Celgard 2500) as the separator, lithium metal anode, and the electrolyte of 1 M $LiPF_6$ and 0.2 M LiDFOB dissolved in FEC and DEC (4:6 by volume). The charge–discharge tests were performed on a typical NEWARE battery test station in the voltage range between 2.0 and 4.7 V with different current densities (1C = 200 mAh g^{-1}). Electrochemical impedance spectroscopy (EIS) was measured using the Solartron 1470 Electrochemical Interface with an amplitude of 5 mV and a frequency range of 0.1 Hz to 1 MHz. After activation of the first cycle at 0.1C, galvanostatic intermittent titration (GITT) experiments were performed with a constant current density of 0.1C for 10 min followed by 40 min relaxation in the voltage range of 2.0–4.7 V.

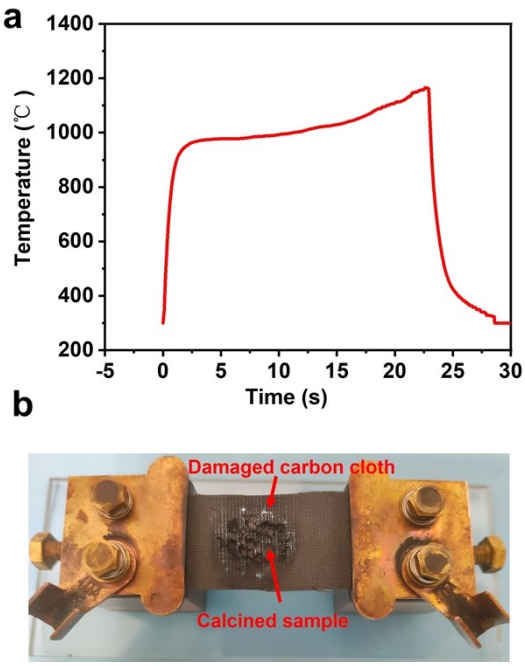

Fig. S1. (a) The temperature versus time curve in the carbon-based Joule heating process and (b) Photograph after the calcination process. In the carbon-based Joule heating process, due to the poor thermal stability of the carbon cloth, the constant temperature lasts only about 12 s after the heating process and the temperature continues to rise afterwards.

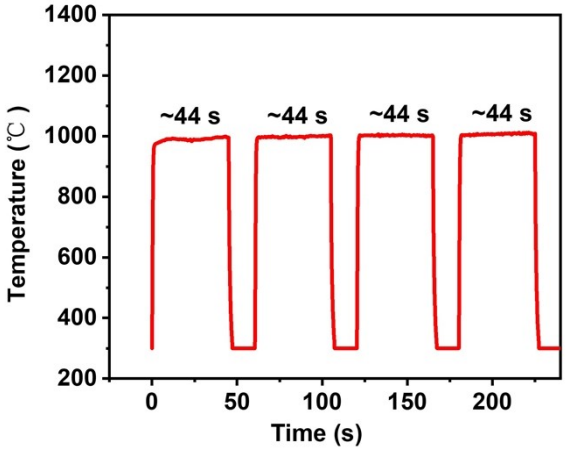

Fig. S2. The temperature versus time curve in the NFTS process. In the NFTS process, due to the excellent thermal stability of the nickel foil, the temperature in the constant temperature zone can be kept almost the same at different cycles, which enables continuous synthesis of KP-LLO.

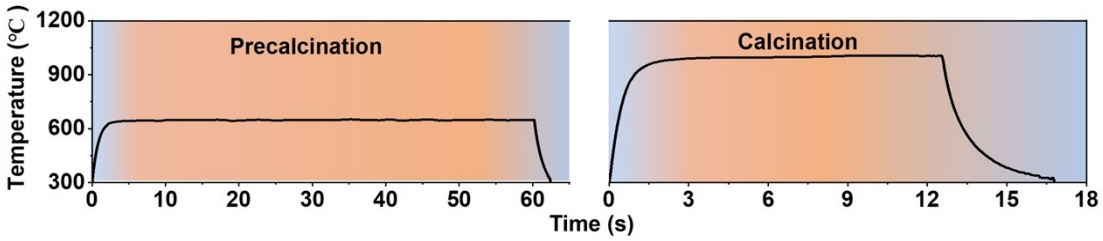

Fig. S3. Temperature curve of the synthesis process of KP-LLO by using carbon-based Joule heating.

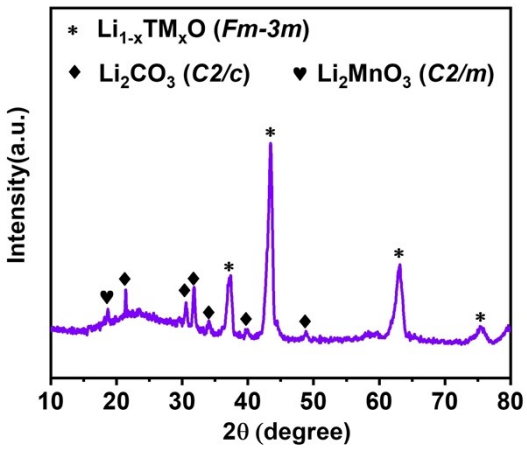

Fig. S4. XRD pattern of the calcined precursor of KP-LLO by using carbon-based Joule heating.

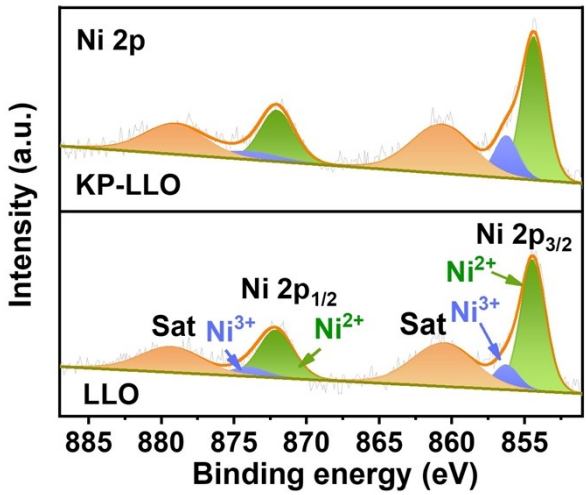

Fig. S5. XPS spectra of Ni 2p for KP-LLO and LLO.

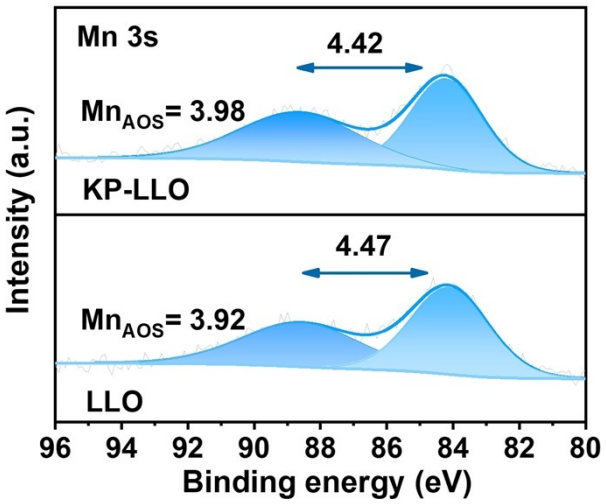

Fig. S6. XPS spectra of Mn 3s for KP-LLO and LLO.

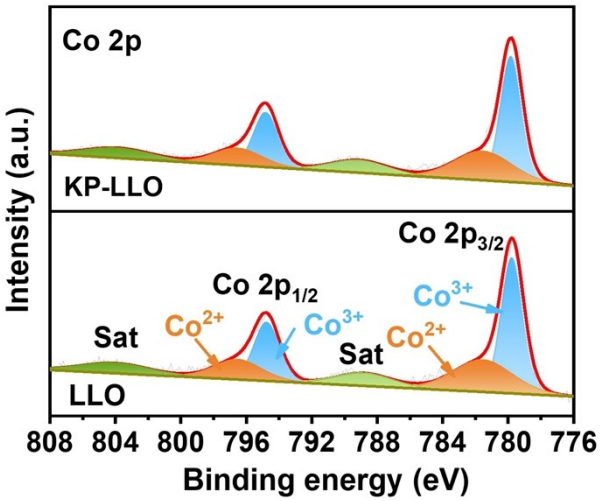

Fig. S7. XPS spectra of Co 2p for KP-LLO and LLO.

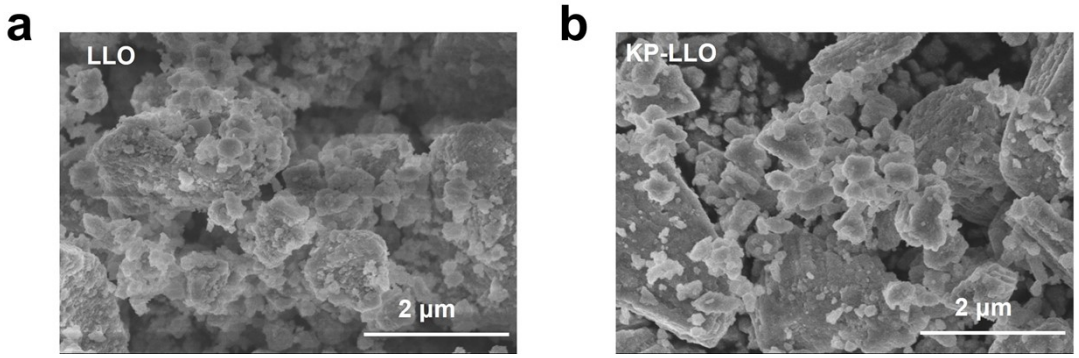

Fig. S8. SEM images for (a) LLO and (b) KP-LLO.

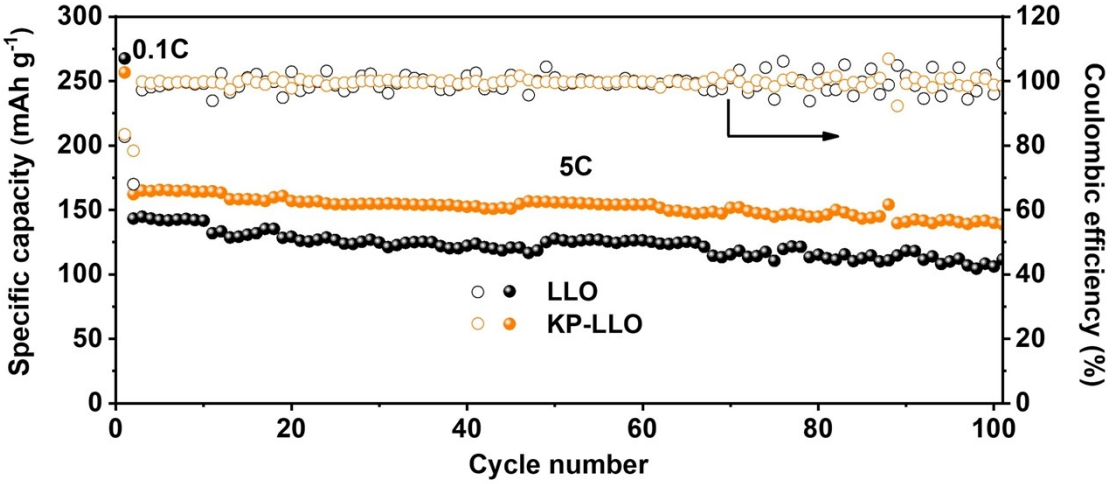

Fig. S9. The cycling performance at 5C after one cycle of activation at 0.1C for KP-LLO and LLO.

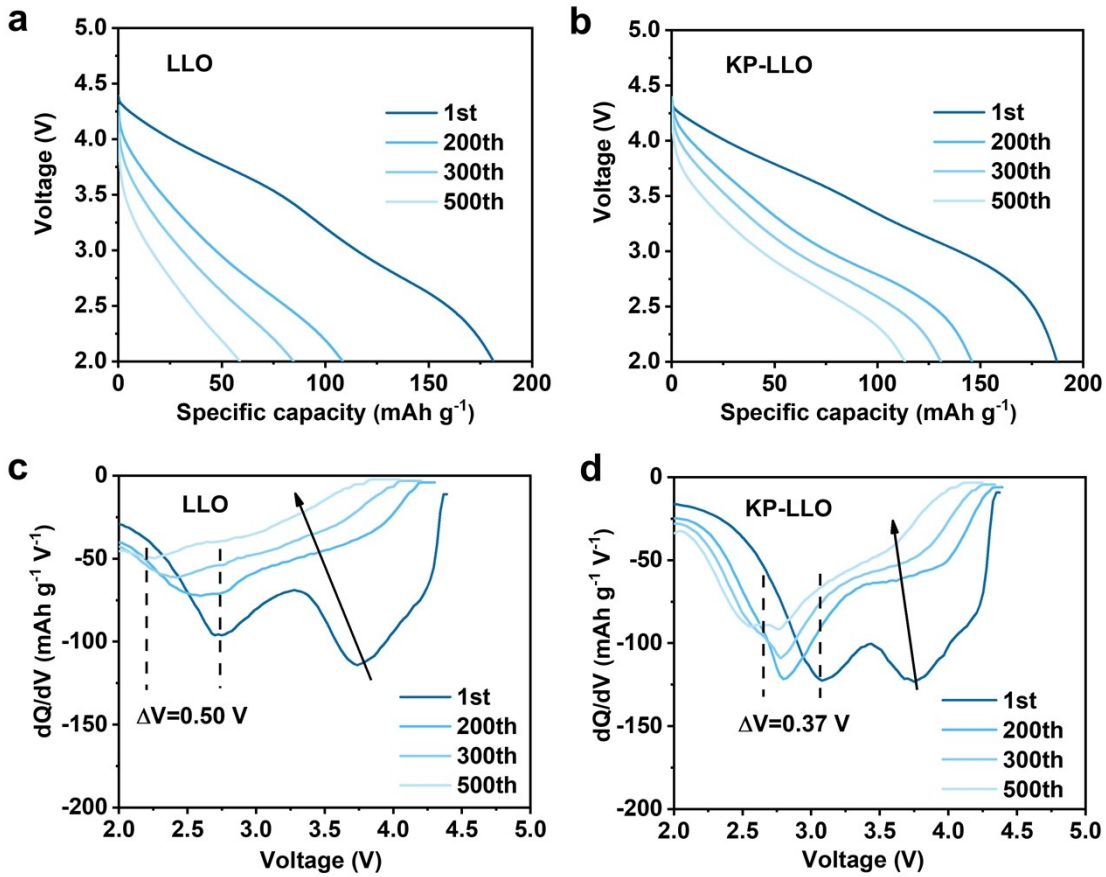

Fig. S10. The discharge curves of (a) LLO and (b) KP-LLO at different cycles at 2C. The corresponding dQ/dV curves of (c) LLO and (d) KP-LLO.

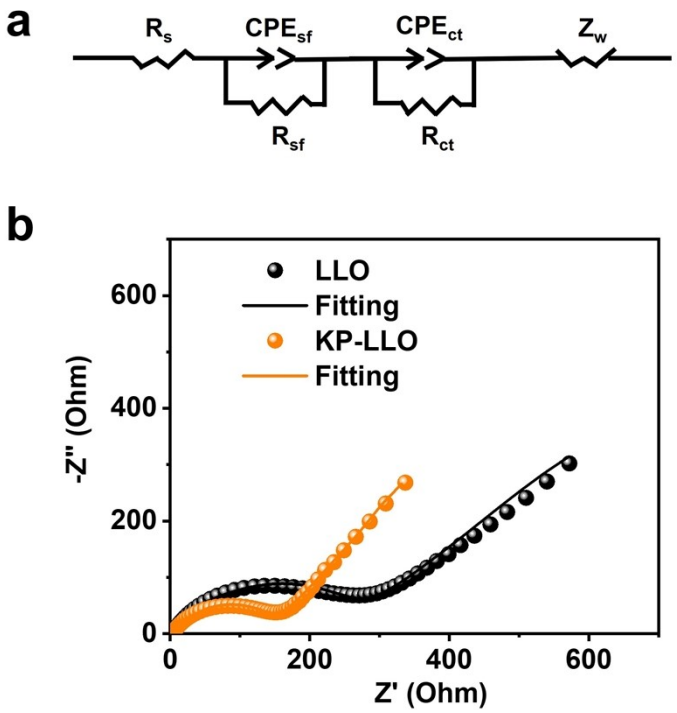

Fig. S11. (a) Equivalent circuit and (b) Nyquist plots after 1cycle at 0.1C for LLO and KP-LLO.

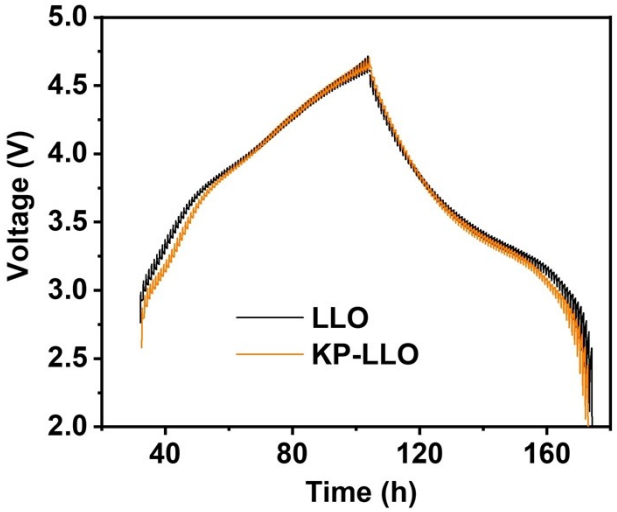

Fig. S12. GITT curves of KP-LLO and LLO for the second cycle at 0.1C.

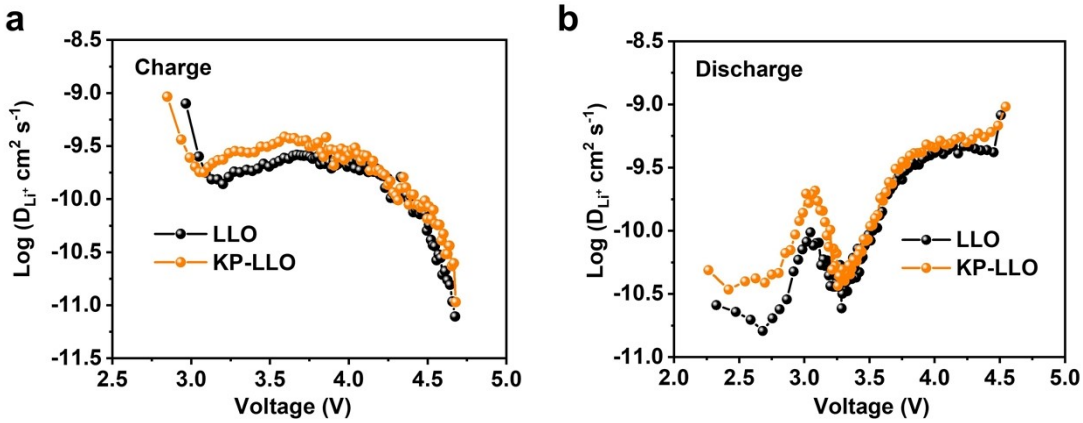

Fig. S13. Li^+ diffusion coefficient in (a) the charge and (b) the discharge process for the second cycle at 0.1C.

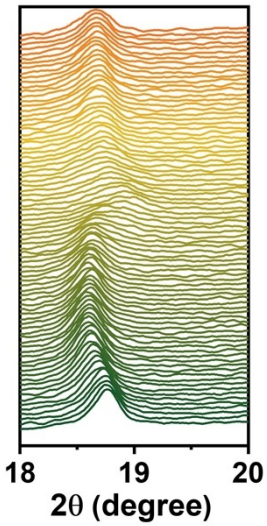

Fig. S14. In situ XRD patterns of LLO during first charge-discharge process.

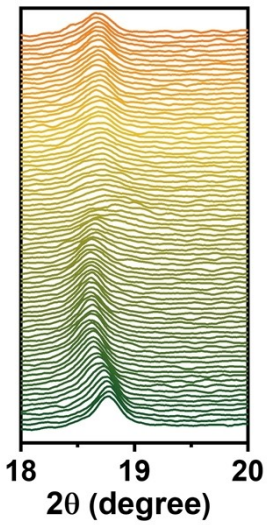

Fig. S15. In situ XRD patterns of KP-LLO during first charge-discharge process.

Table S1. Comparison of calcination time of LLO-based materials.

LLO-based material	Synthesis method	Calcination time (h)	Reference
KP-LLO	NFTS	0.027	This work
$(BO_4)^{5-}$ doping	Sol-gel	19	2
Spinel-like phase coating	Co-precipitation	17	3
Al^{3+} doping	Self-combustion reaction	23	4
Mg^{2+} doping	Co-precipitation	18	5
Surface oxygen vacancies	Co-precipitation and gas–solid interface reaction	30	6
Ru^{4+} doping	Solid-state reaction	15	7

Table S2. ICP-OES results of LLO and KP-LLO.

Sample	Measured molar ratio					
	Li	Ni	Co	Mn	K	P
LLO	1.2035	0.1333	0.1332	0.5411	-	-
KP-LLO	1.1967	0.1325	0.1326	0.5408	0.0101	0.0098

Table S3. Rietveld refinement results of XRD patterns for KP-LLO and LLO.

Sample	LLO	KP-LLO
a (Å)	2.8503	2.8507
c (Å)	14.2326	14.2352
c/a	4.9934	4.9936
V ($Å^3$)	100.1390	100.1800
Ni in Li layer (%)	2.5	11.1
$I_{(LiO2)}$ (Å)[a]	2.2280	2.3906
R_{wp}(%)	8.6	9.4

[a]The Li layer space ($I_{(LiO2)}$) of the layered structure is calculated according to the two equations ($S_{(MO2)} = 2[(1/3) - Z_{ox}]\times c$; $I_{(LiO2)} = (c/3) - S_{(MO2)}$) reported in previous studies.[8] $S_{(MO2)}$ is the slab thickness of the layered structure. Z_{ox} is the oxygen position at 6c sites.

Table S4. Comparison of voltage decay of the reported LLOs.

Modified strategy	Cycle number (n)	Voltage decay (mV / cycle)	Reference

KP-LLO	500	1.1	This work
Ti^{4+} doping	130	3.3	24
Spinel coating	50	4.4	9
Li_3PO_4 and spinel dual coating	100	5.5	25
$LiMgPO_4$ coating	250	1.6	10
$Li_{0.5}Mn_{0.5}O$ coating	200	2.3	26
$Li_4M_5O_{12}$ @LBO dual coating	100	4.8	11
LiF-MgF_2-CaF_2 coating and Mg^{2+}, Ca^{2+}, F^- doping	120	3.1	27
La^{3+} doping	100	1.5	12
Li_2TiO_3 coating	125	1.3	28
CoF_2 coating	100	3.1	13
Surface Al-doping	100	3.1	29
$LiCoPO_4$ and spinel dual coating	100	4.0	14
Surficial oxygen vacancies	200	1.5	30
Nb^{5+} surface doping	100	1.4	15
Li_3PO_4 and spinel dual coating	300	0.8	31
$Li_4Mn_5O_{12}$ coating	300	1.8	16
F^- gradient doping and LiF coating	100	1.75	32
La doping and CaF_2 coating	100	2.0	17
$LiCeO_2$ coating	200	2.0	18
$LiTaO_3$ coating	50	2.2	19
$K_{1-x}Li_xF$ coating and K surface doping	100	3.1	20
CeO_2@Rocksalt surface modification	200	1.8	21
PDA coating	200	1.5	22
Single-crystal LLO	50	2.5	23

Table S5. The fitted impedance parameters of KP-LLO and LLO.

Samples	1st cycle		
	R_s (Ω)	R_{sf} (Ω)	R_{ct} (Ω)
LLO	4.5	55.2	188.6
KP-LLO	4.7	16.9	122.3

Movie S1. The NFTS process.

References

1. B. H. Toby, *J. Appl. Crystallogr.*, 2001, **34**, 210-213.
2. B. A. Li, H. J. Yan, J. Ma, P. R. Yu, D. G. Xia, W. F. Huang, W. S. Chu and Z. Y. Wu, *Adv. Funct. Mater.*, 2014, **24**, 5112-5118.
3. Z. Hao, H. Sun, Y. Ni, G. Yang, Z. Yang, Z. Hao, R. Wang, P. Yang, Y. Lu, Q. Zhao, W. Xie, Z. Yan, W. Zhang and J. Chen, *Adv. Mater.*, 2023, e2307617.
4. P. K. Nayak, J. Grinblat, M. Levi, E. Levi, S. Kim, J. W. Choi and D. Aurbach, *Adv. Energy Mater.*, 2016, **6**, 1502398.
5. R. Z. Yu, X. Y. Wang, Y. Q. Fu, L. W. Wang, S. Y. Cai, M. H. Liu, B. Lu, G. Wang, D. Wang, Q. F. Ren and X. K. Yang, *J. Mater. Chem. A*, 2016, **4**, 4941-4951.
6. B. Qiu, M. H. Zhang, L. J. Wu, J. Wang, Y. G. Xia, D. N. Qian, H. D. Liu, S. Hy, Y. Chen, K. An, Y. M. Zhu, Z. P. Liu and Y. S. Meng, *Nat. Commun.*, 2016, **7**, 12108.
7. Y. M. Fan, E. Olsson, G. M. Liang, Z. J. Wang, A. M. D'Angelo, B. Johannessen, L. Thomsen, B. Cowie, J. X. Li, F. L. Zhang, Y. L. Zhao, W. K. Pang, Q. Cai and Z. P. Guo, *Angew. Chem., Int. Ed.* 2023, **135**, e202213806.
8. A. Rougier, P. Gravereau and C. Delmas, *J. Electrochem. Soc.*, 1996, **143**, 1168.
9. F. Wu, N. Li, Y. F. Su, L. J. Zhan, L. Y. Bao, J. Wang, L. Chen, Y. Zheng, L. Q. Dai, J. Y. Peng and S. Chen, *Nano Lett.*, 2014, **14**, 3550-3555.
10. W. Liu, P. Oh, X. Liu, S. Myeong, W. Cho and J. Cho, *Adv. Energy Mater.*, 2015, **5**, 1500274.
11. X. F. Bian, Q. Fu, H. L. Qiu, F. Du, Y. Gao, L. J. Zhang, B. Zou, G. Chen and Y. J. Wei, *Chem. Mater.*, 2015, **27**, 5745-5754.
12. R. Z. Yu, G. Wang, M. H. Liu, X. H. Zhang, X. Y. Wang, H. B. Shu, X. K. Yang and W. H. Huang, *J. Power Sources*, 2016, **335**, 65-75.
13. S. K. Chong, Y. Z. Chen, W. W. Yan, S. W. Guo, Q. Tan, Y. F. Wu, T. Jiang and Y. N. Liu, *J. Power Sources*, 2016, **332**, 230-239.
14. M. J. Lee, E. Lho, P. Oh, Y. Son and J. Cho, *Nano Res.*, 2017, **10**, 4210-4220.
15. S. Liu, Z. P. Liu, X. Shen, W. H. Li, Y. R. Gao, M. N. Banis, M. S. Li, K. Chen, L. Zhu, R. C. Yu, Z. X. Wang, X. L. Sun, G. Lu, Q. Y. Kong, X. D. Bai and L. Q. Chen, *Adv. Energy Mater.*, 2018, **8**, 1802105.
16. X. D. Zhang, J. L. Shi, J. Y. Liang, Y. X. Yin, J. N. Zhang, X. Q. Yu and Y. G. Guo, *Adv. Mater.*, 2018, **30**, 1801751.
17. M. Li, Y. Zhou, X. Y. Wu, L. Duan, C. M. Zhang, F. Zhang and D. N. He, *Electrochim. Acta*, 2018, **275**, 18-24.
18. Y. Y. Liu, Z. Yang, J. J. Zhong, J. L. Li, R. R. Li, Y. Yu and F. Y. Kang, *ACS Nano*, 2019, **13**, 11891-11900.
19. M. T. Si, D. D. Wang, R. Zhao, D. Pan, C. Zhang, C. Y. Yu, X. Lu, H. L. Zhao and Y. Bai, *Adv. Sci.*, 2020, **7**, 1902538.
20. X. Ding, Y. X. Li, X. D. He, J. Y. Liao, Q. Hu, F. Chen, X. Q. Zhang, Y. Zhao and C. H. Chen, *ACS Appl. Mater. Interfaces*, 2019, **11**, 31477-31483.
21. C. X. Zhang, Y. Z. Feng, B. Wei, C. P. Liang, L. J. Zhou, D. G. Ivey, P. Wang

and W. F. Wei, *Nano Energy*, 2020, **75**, 104995.
22. S. Y. Kim, C. S. Park, S. Hosseini, J. Lampert, Y. J. Kim and L. F. Nazar, *Adv. Energy Mater.*, 2021, **11**, 2100552.
23. J. M. Sun, C. C. Sheng, X. Cao, P. F. Wang, P. He, H. J. Yang, Z. Chang, X. Y. Yue and H. S. Zhou, *Adv. Funct. Mater.*, 2022, **32**, 2110295.
24. Z. X. Yu, S. L. Shang, M. L. Gordin, A. Mousharraf, Z. K. Liu and D. H. Wang, *J. Mater. Chem. A*, 2015, **3**, 17376-17384.
25. S. H. Li, H. X. Li, H. Y. Zhang, S. Zhang, Y. Q. Lai and Z. Zhang, *Chem. Eng. J.*, 2022, **427**, 132036.
26. A. P. Zhu, Q. Wang, Y. Zhang, Y. Y. Zhang, X. G. He, K. P. Wu, H. Wu, Q. Wang, W. L. Cai and Y. Zhang, *J. Energy Chem.*, 2022, **71**, 384-391.
27. H. Zhao, W. T. Li, J. X. Li, H. Y. Xu, C. Zhang, J. Li, C. Han, Z. L. Li, M. Chu and X. P. Qiu, *Nano Energy*, 2022, **92**, 106760.
28. J. D. Liu, Z. H. Wu, M. Yu, H. L. Hu, Y. D. Zhang, K. Zhang, Z. X. Du, F. Y. Cheng and J. Chen, *Small*, 2022, **18,** 2106337.
29. S. W. Li, L. Yang, Z. P. Liu, C. Zhang, X. Shen, Y. R. Gao, Q. Y. Kong, Z. W. Hu, C. Y. Kuo, H. J. Lin, C. T. Chen, Y. Yang, J. Ma, Z. L. Hu, X. F. Wang, R. C. Yu, Z. X. Wang and L. Q. Chen, *Energy Storage Mater.*, 2023, **55**, 356-363.
30. K. Wang, J. M. Qiu, F. C. Hou, M. Yang, K. Q. Nie, J. U. Wang, Y. C. Hou, W. Y. Huang, W. G. Zhao, P. X. Zhang, J. H. Lin, J. T. Hu, F. Pan and M. J. Zhang, *Adv. Energy Mater.*, 2023, **13**, 2301216.
31. W. H. Zeng, F. Liu, J. L. Yang, B. K. Zhang, F. Cao, W. X. Tian, J. Wang, R. H. Yu, F. J. Xia, H. Y. Peng, J. J. Ma, Z. B. Wang, . C. Mu and J. S. Wu, *Energy Storage Mater.*, 2023, **54**, 651-660.
32. L. Di, C. Yufang, S. Weiwei, X. Wei, Y. Shuaiyu, L. Shiqiang, Z. Lanlan, Z. Yanshuang, Y. Tianyan, X. Peitao and Z. Chunman, *Adv. Energy Mater.*, 2023, **13**, 2301765.